Proceedings of ICRC 2001: 2058 © Copernicus Gesellschaft 2001

ICRC 2001

Particle acceleration and synchrotron emission from relativistic blastwaves

T. P. Downes[1], **P. Duffy**[2], **and S. Komissarov**[3]

[1]School of Mathematical Sciences, DCU, Dublin 9, Ireland
[2]Department of Mathematical Physics, UCD, Dublin 4, Ireland
[3]Department of Applied Mathematics, University of Leeds, Leeds LS2 9JT, UK

Abstract. Relativistic blastwaves accelerate particles which are scattered by a highly disordered magnetic field. These particles are then advected downstream of the shock where they emit synchrotron radiation in the ambient magnetic field. We have developed a numerical code to study the hydrodynamics of a strong relativistic blastwave with a general equation of state. We study the acceleration of particles by the forward and reverse shocks and solve for their emission. Implications for the fireball model of gamma ray bursts are discussed.

1 Introduction

Relativistic shock fronts in sources such as Active Galactic Nuclei (AGNs) and fireball models of gamma rays bursts (GRBs) are associated with highly energetic particles inferred through non-thermal emission processes. In this paper we present a one-dimensional, spherically symmetric simulation of a relativistic blastwave propagating into an external medium at rest where both forward and reverse shocks are present. First order Fermi acceleration occurs at such shocks and we model this process and the subsequent synchrotron and adiabatic losses in order to produce light curves which can be expected from such the detailed hydrodynamics. This work is based on recent work contained in Downes, Duffy and Komissarov 2001 (@) (DDK) which contains a more detailed discussion of the model and results.

2 Hydrodynamics

The conservation equations for relativistic hydrodynamics in spherical symmetry are

$$\frac{\partial}{\partial t}\left(\Gamma\rho\right) + \frac{1}{r^2}\frac{\partial}{\partial r}\left(r^2\Gamma\rho\beta\right) = 0 \quad (1)$$

$$\frac{\partial}{\partial t}\left(w\Gamma^2\beta\right) + \frac{1}{r^2}\frac{\partial}{\partial r}\left[r^2\left(w\Gamma^2\beta^2 + p\right)\right] = \frac{2p}{r} \quad (2)$$

Correspondence to: P. Duffy (peter.duffy@ucd.ie)

$$\frac{\partial}{\partial t}\left(w\Gamma^2 - p\right) + \frac{1}{r^2}\frac{\partial}{\partial r}\left(r^2 w\Gamma^2\beta\right) = 0 \quad (3)$$

where Γ is the fluid Lorentz factor, ρ is the proper density, β is the velocity in $c = 1$ units, w is the enthalpy and p is the proper pressure. Time, t, and distance, r, refer to the coordinates measured in the observer's frame. We can relate the enthalpy, density and pressure by

$$w = \rho + \frac{\gamma_*}{\gamma_* - 1}p \quad (4)$$

We employ a second order finite volume Godunov-type scheme on a hierarchical grid to solve the equations 1 to 3. Assuming that the grid cells are defined so that cell i occupies the space $[r_{i-1/2}, r_{i+1/2}]$ then the scheme can be written as

$$\boldsymbol{U}_i^{n+1} = \boldsymbol{U}_i^n - \frac{3\Delta t}{r_{i+1/2}^3 - r_{i-1/2}^3}\left[r_{i+1/2}^2\boldsymbol{F}_{i+1/2}^{n+1/2} - r_{i-1/2}^2\boldsymbol{F}_{i-1/2}^{n+1/2}\right] + \boldsymbol{S}_i^{n+1/2}\Delta t \quad (5)$$

where superscripts refer to the time index and subscripts refer to the spatial index. Also,

$$\boldsymbol{U}_i^n = \left[\left(\Gamma\rho, \Gamma\rho\beta, w\Gamma^2 - p\right)^T\right]_i^n \quad (6)$$

$$\boldsymbol{F}_{i\pm1/2}^n = \left[\left(\Gamma\rho\beta, w\Gamma^2\beta^2 + p, w\Gamma^2\beta\right)^T\right]_{i\pm1/2}^n \quad (7)$$

$$\boldsymbol{S}_i^n = \left[\left(0, \frac{2p}{r}, 0\right)^T\right]_i^n \quad (8)$$

The code has been rigorously tested successfully against various shock-tube problems.

In studies of the fireball model of gamma-ray bursts, the parameters used are the total , M, and the initial radius, R_0. In general, E, the total energy, is thought to lie somewhere in the region 10^{51}-10^{54} ergs. The ratio between the rest-mass energy in the blast (i.e. the mass of the baryonic component), and the total energy determines two critical radii. These are the radius at which the baryons have been accelerated up to their maximum velocity, R_c, and the radius at which

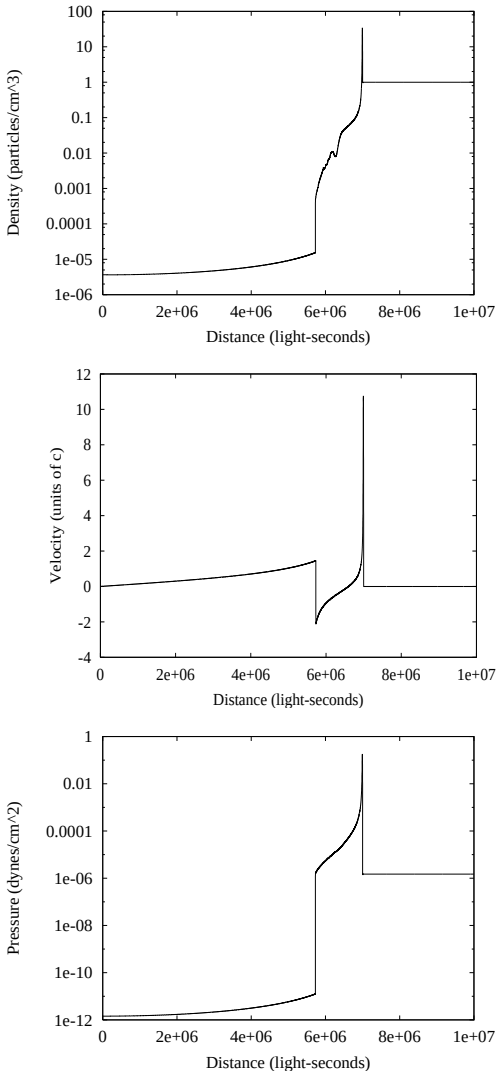

Fig. 1.
Plots of density, 4-velocity and pressure (top to bottom) for a time of 7×10^6 seconds after the initial blast. We can see the original and reflected rarefaction, as well as the forward and reverse shocks.

the shell of ejected baryons have swept up their own mass in interstellar material, R_d. This latter radius is the radius at which the baryonic shell begins to decelerate. The former also depends on R_0, the initial radius of the blast. This initial radius is thought to be quite small, with $R_0 \sim 10^{12}$ cm. The hydrodynamic results presented in figure (1) are for the case $E = 10^{51}$ ergs. The ratio of energy to mass is $\eta = \frac{E}{Mc^2} = 580$ while the initial radius is $R_0 = 1.2 \times 10^{14}$ cm. The presence of forward and reverse shocks is clearly seen in figure (1) and these are the sites of particle acceleration. The qualitative evolution of a spherical relativistic blastwave is discussed thoroughly in DDK.

3 Particle acceleration and losses

Relativistic shocks can accelerate particles by the diffusive shock mechanism under the presence of magnetic fluctuations which enable multiple shock crossings. It has been shown recently (Kirk et al. 2000 (@)) that ultra-relativistic shocks produce a power law distribution of particles with index 2.23, i.e. $N(E) \propto E^{-2.23}$. Therefore, over hydrodynamical timescales we can treat acceleration as an impulsive injection of energetic particles, with this universal power law, into each fluid element which passes through a relativistic shock. Once an electron is injected at the shock it will be scattered in the local fluid frame and suffer both synchrotron and adiabatic losses. If the length scale over which the electrons are isotropised is much shorter than any other length scale of interest then the relativistic electrons will respond adiabatically to the expansion or contraction of the flow. Adiabatic losses, or indeed gains, are then described by the fact that $p/\rho^{1/3}$ is constant where p and ρ are the particle momentum and fluid density in the local fluid frame. With $E = pc$ for ultra-relativistic particles the combined synchrotron and adiabatic losses are described in the comoving frame by

$$\dot{E} = -\alpha B^2 E^2 + \frac{1}{3}\frac{\dot{\rho}}{\rho} E \tag{9}$$

where α is a constant and B the magnetic field strength in the local fluid frame. Consider now a fluid element which is shocked at time $\hat{t}_0$ when a power law distribution of energetic particles is injected and where $\hat{t}$ is time measured in the comoving frame. This population then evolves according to the equation

$$\frac{\partial N}{\partial \hat{t}} + \frac{\partial}{\partial E}\left(\dot{E} N\right) = Q(E, \hat{t}) \tag{10}$$

where $N(E, \hat{t})$ is the differential number of particles of energy E at time $\hat{t}$. The losses, $\dot{E}$, are given by equation (9) while the injection term is $Q(E, \hat{t}) = Q_0 \delta(\hat{t} - \hat{t}_0) H(E - E_{\min}) E^{-q}$ which describes injection of a power law spectrum at time $\hat{t}_0$ with a minimum particle energy $E_{\min}$. We can solve equation (10) by finding the characteristic curves along which $N(E, \hat{t}) dE = N(E_0, \hat{t}_0) dE_0$ where a particle with energy E_0 at $\hat{t}_0$ cools to an energy E at time $\hat{t}$. From equation (9) we have

$$\frac{d}{d\hat{t}}\left(E^{-1} \rho^{\frac{1}{3}}\right) = \alpha \rho^{\frac{1}{3}} B^2 \tag{11}$$

which can be solved to show that along a characteristic curve

$$E_0 = \frac{\rho_0^{\frac{1}{3}} E}{\rho^{\frac{1}{3}} - \alpha E \int_{\hat{t}_0}^{\hat{t}} \rho^{\frac{1}{3}} B^2 d\hat{t}} \tag{12}$$

N is conserved so that

$$\frac{dE_0}{dE} = \frac{\rho_0^{\frac{1}{3}}\rho^{\frac{1}{3}}}{\left(\rho^{\frac{1}{3}} - \alpha E \int_{\hat{t}_0}^{\hat{t}} \rho^{\frac{1}{3}} B^2 d\hat{t}\right)^2} \quad (13)$$

and the solution to (10) becomes

$$N(E,\hat{t}) = Q_0 \rho_0^{\frac{1-p}{3}} \rho^{\frac{1}{3}} E^{-p} \left(\rho^{\frac{1}{3}} - \alpha E \int_{\hat{t}_0}^{\hat{t}} \rho^{\frac{1}{3}} B^2 d\hat{t}\right)^{p-2} \quad (14)$$

In order to calculate the particle spectrum we therefore evaluate the integral in equation (14) for each fluid element which has passed through a shock at some point.

We approximate the emission of a single particle to be a delta function in frequency with a single particle emissivity in the fluid frame given by $j_{\hat{\nu}}(\gamma) = a_0\gamma^2 B^2 \delta(\hat{\nu} - a_1\gamma^2 B)$ where γ is the Lorentz factor of the electron in the fluid frame, $a_0 = \sigma_T c/6\pi$ and $a_1 = e/2\pi m_e c$ with σ_T the Thomson cross section. With the local electron spectrum given by 14, the emissivity in the local fluid frame is then

$$\hat{\mathcal{E}}_{\hat{\nu}} = \int j_{\hat{\nu}}(\gamma) N(\gamma,\hat{t})\, d\gamma \quad (15)$$

The emissivity in the observer's frame is related to that in the fluid frame by $\mathcal{E}_\nu = D^2\hat{\mathcal{E}}_{\hat{\nu}}$. The Doppler factor, D, for the fluid element with a three velocity β making an angle θ to the line of sight is $D = [\Gamma(1-\mu\beta)]^{-1}$ where $\mu = \cos\theta$. The observed frequency is related to the photon frequency in the fluid frame by $\nu = D\hat{\nu}$. The observed flux density flux density is obtained by integrating the intensity over the entire source,

$$F_\nu(t_0) = \int_\Omega \int_0^\infty \mathcal{E}_\nu(s,\phi,t)\, ds\, d\Omega \quad (16)$$

where t_0 is the time of observation and $t = t_0 - s/c$ is the time of emission in the observer's frame a distance s away from the observer

In the simple case where the fluid is assumed to move directly towards the observer with a constant velocity we have succesfully compared our method with the exact results of Sari and Piran 1997 (@). In this instance we succesfully reproduce all the relevant regimes. In particular from those particles which have not radiated away a significant fraction of their energy we get the *uncooled* spectrum of $F_\nu \propto \nu^{-(p-1)/2}$ while the higher energy particles have a steeper, *cooled* spectrum of $F_\nu \propto \nu^{-p/2}$. Below the minimum observed frequency the flux scales as $F_\nu \propto \nu^{1/3}$ as a result of synchrotron self absorption.

4 Spectra and Light Curves

We introduce three parameters in order to implement the particle acceleration model. They are the ratio, ϵ_b, between the magnetic field energy density and the thermal energy density. Secondly, the fraction, ϵ_e, of the downstream thermal energy density which is converted into high energy electrons as a fluid cell is shocked and finally the energy, $E_{\rm min}$, of the lowest energy particle which is produced at the shock. The differential energy spectrum is a power law in energy of index 2.23 from $E_{\rm min}$. The results presented below refer to two different simulations, each using the hydrodynamical results described above. In each case we also have $\epsilon_e = 0.01$. The magnetic field strength is $\epsilon_b = 0.01$ in one simulation, and $\epsilon_b = 0.1$ in the other. This is the only way in which the two simulations differ.

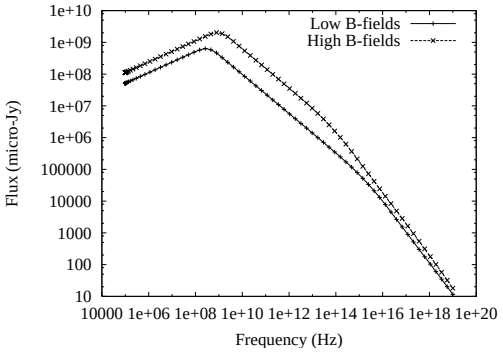

Fig. 2.
The spectrum observed at 1 hr after the inital blast observation for the case of $\epsilon_b = 0.01$ ("Low B-fields") and $\epsilon_b = 0.1$ ("High B-fields")

Figure 2 shows a plot of the spectrum observed 24 hours after the initial blast could have been observed for the case where $\epsilon_b = 0.1$ (hereafter referred to as the high ϵ_b case) and for $\epsilon_b = 0.01$ (hereafter referred to as the low ϵ_b case). In both cases the spectrum is a broken power-law. In the first section of the spectra, the flux goes as $\nu^{1/3}$, as expected for synchrotron radiation below the peak frequency of the lowest energy electron. The second part of the spectrum is, in both cases, the power law $\nu^{-0.615}$ indicating that this part of the spectrum is dominated by emission from electrons, with a distribution of $E^{-2.23}$, which have not suffered significant adiabatic or synchrotron cooling. The break from this part of the spectrum to the final, steeper, part occurs in different places in the spectra plotted. For the high ϵ_b case, the break occurs at a lower frequency than for the low ϵ_b case as would be expected since, in higher magnetic fields, the losses suffered are correspondingly higher. However, while in the final part of the spectrum the exponent predicted from simple theory would be $-p/2 = -1.115$ we find the spectrum to be slightly harder. In the high ϵ_b case, we have $F_\nu \propto \nu^{-1.019}$, and in the low ϵ_b case, $F_\nu \propto \nu^{-0.981}$. The reason for the slightly harder spectra at high frequencies is the non-uniform velocity distribution in the "shell" of ejected material (see, e.g. Figure 1). where material moving at high velocity towards the observer will be more heavily weighted in the spectra than material moving at lower velocity, due to relativistic beaming. The temporal behavious of the break frequencis is

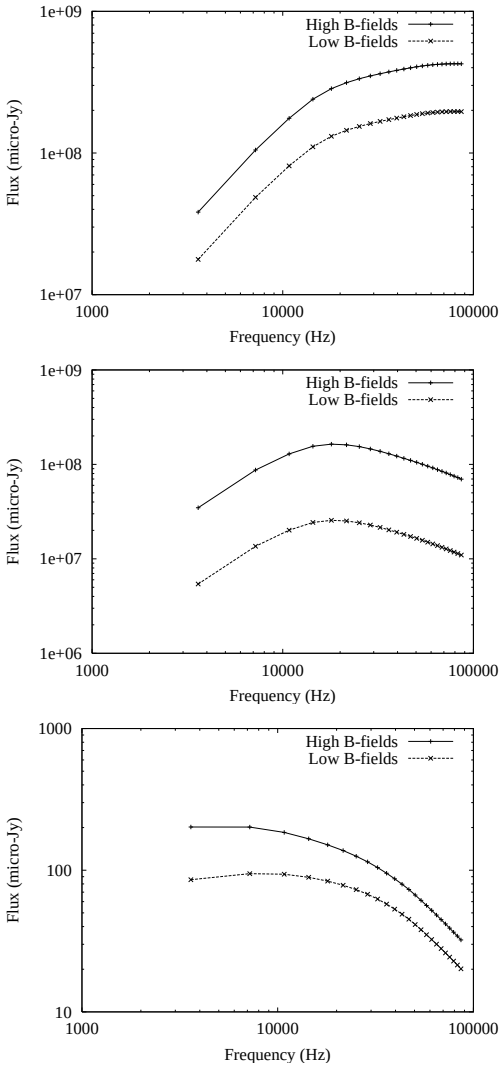

Fig. 3.
Light curves calculated at low, intermediate, and high frequencies.

discussed in DDK.

Figure 3 shows plots of the light curves at low, medium and high frequencies. These frequencies are chosen so that the points are always in the regime where $F_\nu \propto \nu^{1/3}$ (low frequencies), $F_\nu \propto \nu^{\frac{1-p}{2}}$ (medium frequencies) and, for high frequencies, the frequency is always in the third section of the spectrum. Initially we see an increase in all the light curves shown, with the exception of the high frequency, high ϵ_b case, where the emission is roughly constant over the first couple of hours. The medium frequency light curves initially increase and then fall off dramatically. Ags with the high frequency light curves, it is difficult to see any point at which the behaviour of the light curve is a true power-law. The high frequency light curves also begin to fall off very steeply, and again, it is difficult to see any sign of a power-law behaviour in the curves. The lack of a clear power-law behaviour in the light curves may well be due to the restricted time-scale over which the curves are calculated (from 1 hour to 1 day). However, it is clear that, if there is a broken power-law behaviour then the breaks are smeared out, and, in addition, the final fall-off of the light-curve would seem to be much faster than previously predicted. Both of these facts, certainly at high frequencies, are likely to arise from the inclusion of adiabatic cooling in the model. This cooling affects the way the critical frequencies behave, and hence the behaviour of the light curves. Since the second (upper) break frequency decreases faster in the presence of adiabatic cooling, we would expect the high frequency light curve to fall off more rapidly.

5 Conclusions

We have presented a model for the synchrotron emission of energetic particles downstream of relativistic, spherical shock waves. The hydrodynamical part of the problem has been solved numerically with the simpler simulations agreeing with results published elsewhere. On the other hand the particle acceleration aspect has been treated as an *injection* process with relativistic shocks leaving a population of energetic particles immediately downstream. The spectral index is known from semi-analytic work so that we need only specify the fraction of the downstream thermal energy which is converted into energetic particles and a lower cut-off energy. The particles subsequently lose energy by synchrotron cooling and adiabatic losses. The hydrodynamical results have captured the evolution of both the forward and reverse shocks which are of principal interest for particle acceleration and radiative emission as well as the rarefaction waves. The spectra emitted from our system largely agree with the simple predictions for the low energy, uncooled part of the spectrum. However, at the higher, cooled part of the electron population the relativistic boosting of the material coming straight towards the observer hardens the spectrum from the pure uncooled value which comes from material further downstream and from material which is not moving driectly towards the observer. Further non-trivial behaviour has been found for the temporal variation of both the break frequencies and the light curves.

Acknowledgements. This work was supported by the TMR programme of the EU under contract FMRX-CT98-0168.

References

Downes, T.P., Duffy, P., Komissarov S., 2001, MNRAS (submitted) astro-ph0102271
Falle S.A.E.G., Komissarov S., 1996, MNRAS, 278, 586
Kirk J.G., Duffy P., 1999, J. Phys. G, 25, R163
Kirk J.G., Guthmann A.W., Gallant Y.A., Achterberg A., 2000, ApJ, 542, 235
Sari R., Piran T., 1995, ApJ, 455, L143
Sari R., Piran T., 1997, ApJ, 485, 270